Sea ice interannual variability and sensitivity to fall oceanic conditions and winter air temperature in the Gulf of St. Lawrence, Canada.

Peter S. Galbraith[1], Caroline Sévigny[2],
Daniel Bourgault[3], and Dany Dumont[3]

[1]Fisheries and Oceans Canada, Québec Region, Maurice Lamontagne Institute, P.O. Box 1000, Mont-Joli,
Qc, Canada, G5H 3Z4
[2]Environment and Climate Change Canada, 801-1550 avenue D'Estimauville Québec, Qc, G1J 0C3
[3]Institut de sciences de la mer de Rimouski, Université du Québec à Rimouski, 310 allée des Ursulines,
Rimouski, Qc, Canada G5L 3A1

Key Points:

- First occurrence of sea ice in the northwest Gulf of St Lawrence is predicted by air temperature with about 40 days of lead time.
- Seasonal sea ice severity metrics (duration, maximum area and volume) are shown to be related to winter air temperatures.
- The only five nearly ice-free winters correspond to the warmest winter air temperatures over the Gulf.

Corresponding author: Peter S. Galbraith, `Peter.Galbraith@dfo-mpo.gc.ca`

Abstract

The Gulf of St. Lawrence has been nearly free of sea ice five times in its recorded history, three of which have occurred since 2010. This study examines the inter-annual variability of sea ice cover characteristics (1969-2023) and winter mixed layer heat content (1996-2023), their sensitivity to fall oceanic conditions (since fall of 1995) and to winter air temperatures. The study finds no relationship between the first occurrence of sea ice, maximum seasonal volume or winter mixed layer heat content and fall oceanic conditions as determined by the heat content of the water column in early fall. However, it shows that the first occurrence of sea ice in the northwestern Gulf is related to the timing of sea surface temperature crossing the $0°C$ threshold with a lag time of about 3 weeks, and with air temperature dropping below $-1.8°C$ with a lag of roughly 40 days. The average air temperature over the Gulf between December and February or March is highly correlated to seasonal maximum sea ice area and volume, as well as ice season duration. This is likely through a link with sensible heat flux. The five nearly ice-free winters correspond to the warmest December to February (or December to March) average air temperatures over the Gulf. From this is inferred that a warming of 2.2 to $2.4°C$ above the 1991-2020 climatology leads to nearly ice-free conditions in the Gulf of St. Lawrence. This finding is consistent with numerical simulation studies.

Plain Language Summary

The first occurrence and seasonal severity of sea ice in the Gulf of St Lawrence are shown to not be related to early fall ocean conditions. Atmospheric conditions prevalent when water temperature approaches the freezing point are drivers of first occurrence and can be used to predict onset of sea ice in the northwest Gulf with about 40 days of lead time. Seasonal sea ice severity metrics (duration, maximum area and volume) are shown to be related to winter air temperatures. Five nearly ice-free winters correspond to the warmest December to February (or December to March) average air temperatures over the Gulf, providing the threshold required for future climate warming to result in a nearly ice-free Gulf of St. Lawrence of 2.2 to $2.4°C$ above the 1991-2020 climatology.

1 Introduction

The Gulf of St. Lawrence is a close second to the Sea of Okhotsk for having the southernmost sea ice in the northern hemisphere (Takahashi et al., 2011). Being at the southern edge of sea ice extent means that the GSL is particularly sensitive to global warming given the drastic possibility that it eventually becomes completely ice-free year round. The entire area of the Gulf can become ice covered before the end of the severest winters, while less than a quarter of the area is ice covered by the end of mild winters, usually limited to shallow portions of the Gulf such as the Northumberland Strait. Using this threshold of a quarter of the area covered by ice of stage 4 (grey ice of 10-15 cm in thickness) or greater, the Gulf has been nearly ice-free by the end of winter five times in recorded history, with three occurrences since 2010 (as will be shown below). This suggests that climate warming may have already begun to affect sea ice duration, seasonal maximum area and volume in the Gulf, as the long term warming trend added to strong interannual variability has led to more common nearly ice-free winters. The study of the forcing thresholds responsible for similar events is not only relevant, but urgent.

In the high Arctic, predictions of seasonal sea ice outlooks often focus on the melt season and ice breakup dates for navigation and industrial activity purposes (Blockley & Peterson, 2018), and to track the progession towards the September minimum that is expected to become ice-free on occasion within 30 to 50 years (Notz & SIMIP Community, 2020; Bonan et al., 2021). The focus is towards the opposite of forecasting the date of first occurence and of upcoming maximum sea ice conditions at lower latitudes
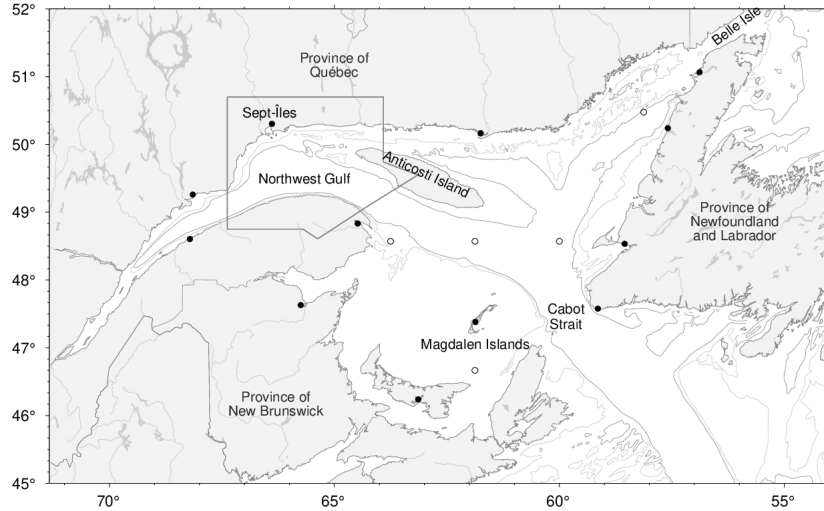
Figure 1. Gulf of St. Lawrence. Thirteen weather stations operated by Environment and Climate Change Canada (ECCC) are shown as black dots. NCEP2 grid points are shown as open circles. The area delimiting the Northwest Gulf is outlined. Isobaths for 100 m and 200 m are shown.

such as the Barents Sea (Arthun et al., 2021), Greenland Sea, and the Sea of Okhotsk (Takahashi et al., 2011).

In the Gulf of St. Lawrence, the interest in seasonal forcasting lies in aid to maintaining the St. Lawrence seaway open for shipping but also to help plan tourism operations such as the observation of harp seal pups on the sea ice. These observations require sea ice floes of sufficiently large size and thickness to safely land a helicopter with tourists. One major such tourism operator reports cancelling five seasons between 2010 and 2023 because of weak sea ice conditions. Climate predictions are of interest to know when the Gulf will become completely ice-free. The topic of inter-annual variability of sea ice in the Gulf of St. Lawrence and its relationship to atmospheric forcing and initial ocean state was examined three decades ago using statistical analysis (Déry, 1992), numerical modelling (DeTracey, 1993), and a combination of both (Li, 2000) in studies that pre-dated the three recent nearly ice-free winters. Li (2000) found that observations of inter-annual variability in December to April surface air temperature accounted for 40% of the variance in sea ice area, but did not provide the linear relationship. Based on the coupled ice-ocean numerical model of Saucier et al. (2003), Senneville and Saucier (2007) found that an increase in winter air temperature of 2°C resulted in a forecasted reduction of 28% in area and 55% in volume of sea ice relative to the period 1996-2003. More recent numerical modelling has also been used to predict sea ice cover under various climate change scenarios. Brickman et al. (2016) and Lavoie et al. (2020) show maps of projected average conditions, but don't delve into the details of the relationship to atmospheric forcing; Brickman et al. (2016) model a nearly ice free Gulf by 2075 under RCP8.5 forcing, while Lavoie et al. (2020) reaches the same conditions by 2061-2080 under RCP8.5 forcing for two of three Earth System Models used for atmospheric downscaling. Long et al. (2016) obtained a crossing of the interannual mean sea ice conditions through zero by 2069 with the increase in winter air temperature of 2 to 3°C. Operational models are also used for sea ice forecasting in the Gulf on the time scale of days (Pellerin et al., 2004; Smith et al., 2013).

Sea ice production is related to ocean mixed layer dynamics and to winter atmospheric conditions (air temperature, winds). The more dominant factor regionally depends on the heat content within the mixed layer, and therefore also its depth, versus the strength of the ocean-atmosphere heat flux. The summertime water column in the Gulf of St. Lawrence consists of three distinct layers: the surface layer, the cold intermediate layer (CIL), and the deeper water layer. Surface temperatures typically reach maximum values in early to mid-August (Galbraith et al., 2012). Gradual cooling occurs thereafter, and wind-forced mixing during the fall leads to a progressively deeper and colder mixed layer, eventually encompassing the CIL. During winter, the surface layer thickens partly due to buoyancy losses (cooling and reduced runoff) and brine rejection associated with sea ice formation, but mostly due to wind-driven mixing prior to ice formation (Galbraith, 2006). The surface winter layer extends to an average depth of 75 m, but may reach >150 m in places such as the Mécatina Trough where near-freezing waters from the Labrador Shelf entering through the Strait of Belle Isle may extend from the surface to the bottom, in depths >200 m (Galbraith, 2006; Shaw & Galbraith, 2023). This winter mixed layer depth is greater than values in most of the Arctic, comparable to the Eurasian Basin, but less than half that of the Barents Sea (Peralta-Ferriz & Woodgate, 2015) or the Labrador Shelf as jugded from the summer Cold Intermediate layer thickness (Cyr et al., 2022). This mixed layer must entirely reach near-freezing temperatures for sea ice to be produced, favoring sea ice formation first in shallow areas where the mixed layer reaches the bottom, or in the Estuary where the stratification limits the mixed layer to shallow depths, and suggesting that ocean heat content should play a large role in seasonal sea ice variability because of the large mixed layer depth and warm fall conditions compared to the Arctic. Restratification occurs in spring with sea ice melt waters and continental runoff lowering surface salinity, combined with surface warming. Underneath this surface layer, cold waters from the previous winter become partly insulated from the atmosphere and form the summer CIL. This layer persists until the next winter, gradually warming up and deepening during summer (Gilbert & Pettigrew, 1997; Cyr et al., 2011), and more rapidly during the fall as vertical mixing intensifies. The deep layer underneath is mostly unaffected by seasonal exchanges with the atmosphere and is not considered here since it is not involved in sea ice production.

This work addresses whether the interannual sea ice variability in the Gulf of St. Lawrence is driven by the atmosphere or by pre-existing conditions of the ocean. It first analyses sea ice data to provide climatologies of sea ice phenology and time series of sea ice season duration and maximum volume and area. It analyses winter hydrographic data to show the mixed layer conditions present during extreme cases of sea ice cover, and fall hydrographic data to determine if early-fall mixed layer conditions explain the variability. The Gulf of St. Lawrence is a rare case study for which the water column under an ice-covered sea is sampled at the end of winter, permitting the evaluation of the mixed layer thickness that had to be cooled to near-freezing before sea ice could be produced. The work briefly considers how far ahead in time upcoming seasonal ice conditions can be forecasted. It identifies relationships between winter atmospheric forcing and observed seasonal extreme sea ice conditions, and seeks to determine if these relationships can be used to infer changes expected from future climate scenarios.

2 Materials and Methods

Ice cover area, duration, and volume are estimated from ice cover products obtained from the Canadian Ice Service (CIS), and further processed onto a regular grid used in analyses. These are weekly Geographic Information System (GIS) charts covering the period 1969-2023. All charts are gridded on a 0.01° latitude by 0.015° longitude grid (approximately 1 km resolution). Thickness (and therefore volume) is estimated from stages of ice growth whether it is new ice (5 cm), nilas (5 cm), grey ice (12.5 cm), grey-white ice (22.5 cm), thin first-year ice (50 cm), medium first-year ice (95 cm) and thick first-

year ice (160 cm). Prior to 1983, the CIS reported ice categories into fewer classifications using a single category of first-year ice (≥ 30 cm) with a suggested average thickness of 65 cm. This value was found to underestimate the seasonal maximum thickness and volume based on high inter-annual correlations obtained between the estimated volume and area of the weekly seasonal maxima. The comparison of areas and volumes pre- and post-1983 provided an estimate of 85 cm, which is used instead of 65 cm.

The surface layexor temperature conditions of the Gulf are monitored by complementary methods. First, three high-resolution satellite-based products are blended to produce weekly composites that cover the area from 1982 to 2023 (Galbraith et al., 2021, 2023). Second, to extend coverage during the sea ice season, a shipboard thermosalinograph consisting of temperature-salinity sensors (SBE-21; Sea-Bird Electronics Inc., Bellevue, WA) has been installed on various commercial ships of Oceanex Inc. since late 1999 (Galbraith et al., 2002). These ships transit between Montréal (Qc) and St. John's (NL) with weekly return trips, crossing the Gulf each time.

Heat flux data and daily surface air temperature were extracted from the NCEP Reanalysis 2 open dataset, provided by the NOAA/OAR/ESRL Physical Sciences Laboratory (Boulder, Colorado, USA) for 1990 to May 2023.

Air temperatures come from the 2023 version of the second generation of homogenized surface air temperature dataset, which is part of the Adjusted and Homogenized Canadian Climate Data (AHCCD), and accounts for shifts due to the relocation of stations, changes in observing practices, and automation (Vincent et al., 2012). Thirteen coastal stations located around the Gulf are used (Figure 1). Monthly temperature climatologies are computed at each station for the period 1991-2020, and then averaged to obtain a spatial average seasonal cycle for the Gulf. Gulf average monthly air temperature anomalies are computed as the average anomalies at all available stations, and seasonal (DJF or DJFM) anomalies are computed as the average of these Gulf average monthly anomalies.

Fall water column temperature and salinity conditions were obtained from Fisheries and Oceans Canada Atlantic Zone Monitoring Program (AZMP) fall surveys (Therriault et al., 1998; Galbraith et al., 2023) using a Sea-Bird Electronics SBE-9/11 CTD probe. The survey dates have shifted from early December to mid-October/mid-November starting in 2002.

Winter mixed layer conditions have been sampled at the end of winter, in the first half of March, since 1996 using helicopter-based oceanographic surveys that is now also part of the AZMP. During these operations, a Sea-Bird Electronics SBE 19plus is lowered from the air to 200 m depth (or the sea floor in shallower areas) while the helicopter maintains a stationary flight, or through an augered ice hole once the aircraft lands on the ice. The first nine years of data collected from these surveys are described in Galbraith (2006), and 28 years of data (1996-2023) are used here.

3 Sea ice metrics climatology and interannual variability

Weekly ice charts were used to grid the day-of-year of the first and last ice occurrences for each season, as well as the duration defined by the number of weeks that sea ice is observed at a grid point. Figure 2 shows the WMO standard 30-year climatology for these metrics, from 1991 to 2020 (WMO, 2017). Ice typically forms first in December in the upper Estuary, on the banks of the St. Lawrence Estuary, and in shallow waters along New Brunswick, Prince Edward Island, and the lower north shores. It melts last in the northeast Gulf where the ice season duration tends to be longest, apart from shallow bays elsewhere. Offshore sea ice is typically produced in the northern parts of the Gulf and drifts towards the Magdalen Islands and Cabot Strait during the ice season (Saucier et al., 2003; Urrego-Blanco & Sheng, 2014).
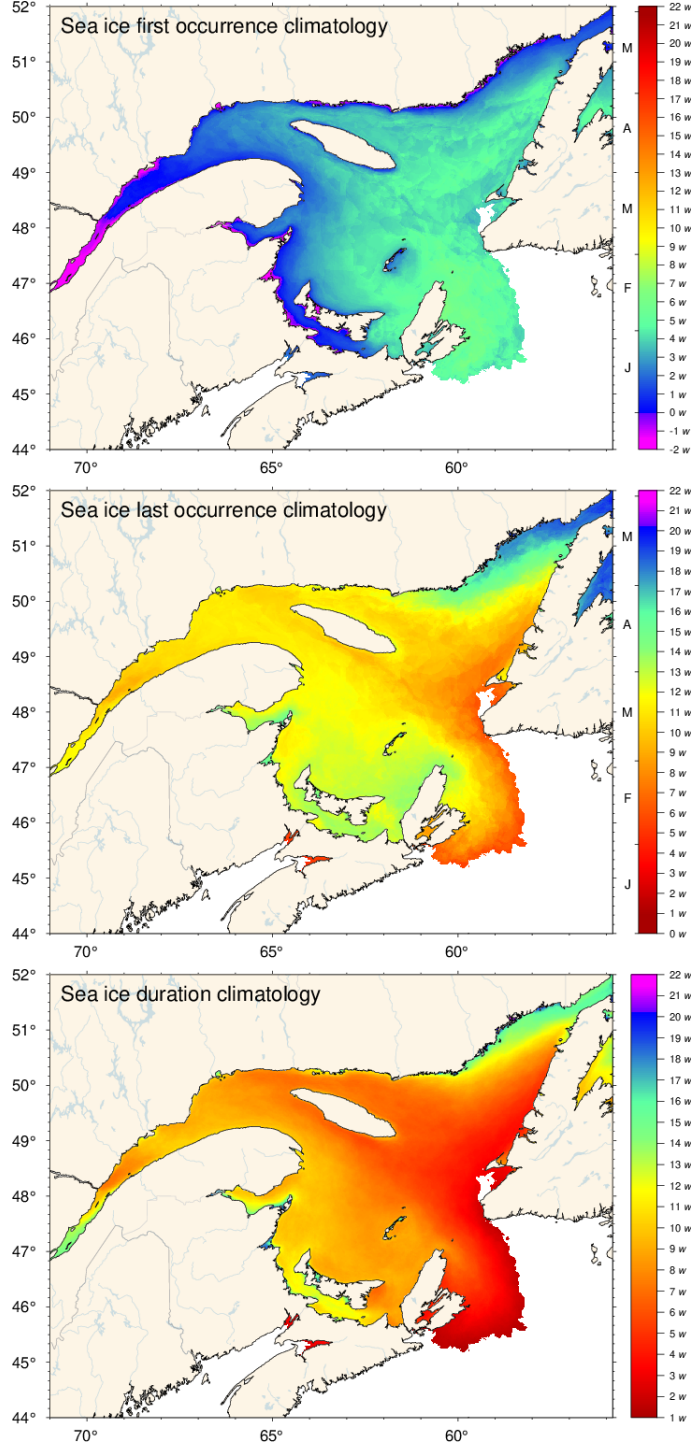
Figure 2. Sea ice phenology climatologies (1991-2020) for the first and last ice occurrence, and ice season duration based on weekly data. The first and last occurrences are defined here as the first and last weekly chart in which any amount of ice is recorded for each pixel, and are shown as day-of-year (DOY). Ice duration sums the number of weeks with ice cover for each pixel. Climatology is shown for pixels with at least 15 of the 30 years with sea ice, and therefore also displays the area where there is 50% probability of having sea ice for at least one week in a given year.

Figure 3 shows the 1991-2020 climatology of ice thickness distribution during the week of maximum seasonal volume, as well as the maximum weekly cover observed in 2003 and 2010, respectively the years of maximum and minimum volume over the 1969-2023 period, and 2016, which is the threshold year discussed later. It also shows the winter surface mixed layer temperature and depth for the same years obtained from the March oceanographic surveys (discussed later). Figure 4 presents the time series of seasonal maximum ice volume, area (excluding thin new ice), and ice season duration in relation to the December to March air temperature anomaly. Ice season duration is calculated from the average of grid points shown in Figure 2, with zeros included when there is no ice in a given year but some are found in the 30-year climatology.

As demonstrated by these two figures, sea ice cover can vary from an almost complete cover shore-to-shore to almost no cover at all, and is tied to mixed layer conditions as surface waters have to reach freezing temperatures throughout the entire mixed layer depth to permit sea ice formation. The total area of the Gulf represents 220 000 km^2 and this area of sea ice is reached during the most severe winters (Note that the area in Fig. 4 includes drift onto the Scotian Shelf). For the purpose of this work, we define a "nearly ice free" Gulf as a maximum seasonal area of less than 1/4 of this value, although the estimated volumes will be less than a quarter than in severe winters because the ice will also be thinner during mild winters. This criterion picks out 1969, 2010, 2011 and 2021 in our dataset as nearly ice free.

In 2010, the mixed layer failed to reach near-freezing by early March everywhere except close to the Strait of Belle Isle, preventing widespread sea ice occurrence. This contrasts with 2003 when the mixed layer was near-freezing over the entire Gulf area in early March. The climatology shows an area near the Eastern end of Cabot Strait where waters are often warmer than freezing; this is an area often devoid of sea ice, such as in 2016. The size of this warm area is highly variable from year-to-year, extending north past the tip of Anticosti Island in 2016. The nearshore zone of the Eastern end of Cabot Strait remains ice-free in the climatology (top left panel), indicating open water conditions during at least 50% of winters.

4 Relation to fall ocean heat content

Since the fall mixed layer temperature must reach the freezing point before sea ice can form, the fall heat content was hypothesized to be decisive for the date of the first occurrence of sea ice in the Gulf of St. Lawrence. The fall oceanographic survey carried out by Fisheries and Oceans Canada was historically called the *ice forecast cruise*, when it was usually carried out in December. In the 1990s, collected temperature-salinity profiles were sent to the Canadian Ice Service for comparison to prior years of observations to serve as input for the seasonal sea ice outlook. This nickname has remained even though the survey has usually been conducted in October for the past 20 years or so. With the benefit of hindsight, this hypothesis can and is hereby tested.

To test whether the fall heat content obtained from surveys conducted in December (before 2002) and October (after and including 2002) has any predictive ability for the first appearance of sea ice, the mixed layer depth measured at each station for each March sampling was first interpolated over the area of the Gulf (e.g. Figure 3). The mixed layer depth is defined here as the depth where salinity is 0.3 greater than the deepest water with $T < -1°C$, or of the coldest water if no waters with $T < -1°C$ are present (which occurs throughout the Gulf in 2010). The addition of 0.3 only serves to extend the mixed layer to the sharp halocline usually present beneath the mixed layer and the ad hoc value of 0.3 is not consequential to the results. The mixed layer depth was then integrated horizontally, providing the mixed layer volume whose heat content was estimated referenced to the freezing point, as a function of the interpolated value of surface salinity. In the following, the heat content will be displayed in ExaJoules (EJ or $\times 10^{18}$ J)
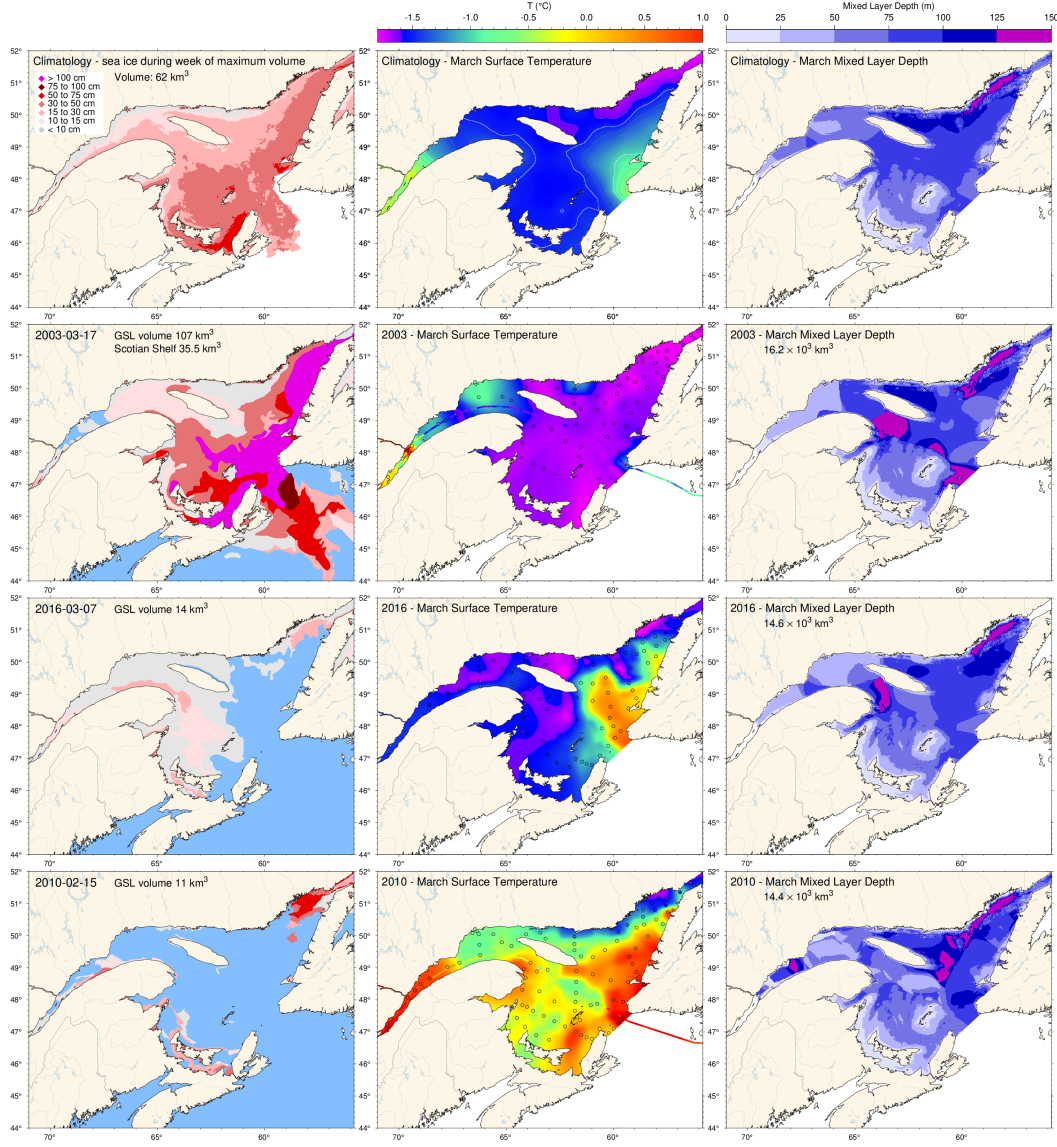
Figure 3. Sea ice thickness distribution during week of maximum seasonal volume, sea surface temperature and mixed layer depth during the early March survey. On the left panels, sea ice thickness for the 1991-2020 climatology, and years 2003 (year of maximum volume), 2016 (threshold year), and 2010 (year of minimum volume). On the middle panels, sea surface temperature interpolated from March survey stations for the 1996-2020 climatology and years 2003, 2016, and 2010, with station locations indicated by circles on the annual maps. Circles are color-coded according to observed temperature and a shipboard thermosalinograph transect is superimposed on the 2003 and 2010 maps. On the right panels, mixed layer depth interpolated from March survey stations for the 1996-2020 climatology and years 2003, 2016, and 2010. Integrated volumes are indicated.
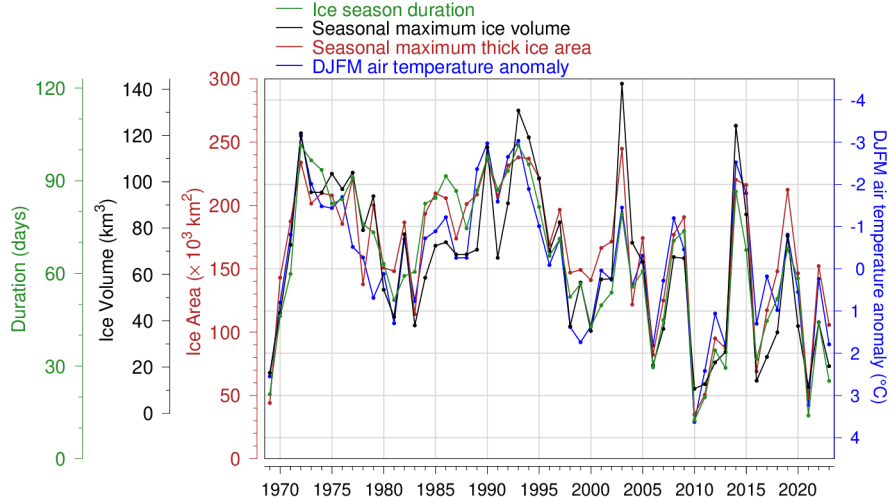
Figure 4. Seasonal maximum ice volume and area including the portion on the Scotian Shelf (area excludes ice less than 15 cm thick), ice season duration, and December to March air temperature anomaly. Mean duration obtained as the spatial average of Fig. 2, excluding the Scotian Shelf, with zeros counted if no ice is present but the 1990-2020 climatology has some. Linear relations indicate losses of 18 km^3, 31000 km^2 and 14 days of the sea ice season for each 1°C increase in winter air temperature (R^2 of 0.75, 0.81, and 0.83 respectively).

and in units of km^3 °C for simplicity, omitting negligible variations of density and specific heat capacity of water. Finally, the March mixed layer depth grid was transposed to the preceeding fall observations and the fall heat content was calculated over the same volume.

The average day-of-year of the first ice occurrence cannot be calculated with a simple average of seasonal grids such as in Figure 2. This would lead to biased estimates due to spatial disparity in the date of first occurrence and interannual variability in sea ice extent; e.g., the sea ice cover extends further out to Eastern Cabot Strait in winters of high sea ice, where the first occurrence is later. Instead, the spatial anomaly grid was calculated for each ice season, relative to the 1991-2020 climatology of the first occurrence, and the spatial average anomaly obtained from this grid is used. Figure 5 (top panel) shows the time series for the average anomaly of first ice occurrence for 1996-2023 and the heat content of the previous fall, i.e. 1995-2022. No statistical relationship is found between these two series, either using the full sequences or excluding 1996-2002 when the preceding fall survey was done in December (R^2 of 0.03 and 0.02 respectively), or even using the short series of 1996-2002. The fall heat content has a statistically significant warming trend but the day-of-year of first occurrence does not. Furthermore, the two years with the latest first sea ice occurrence (2021 and 2011) did not follow a high fall heat content (although the 3rd, 2023, did) nor did the three post-2002 years with the earliest first occurrence (2014, 2019 and 2009) coincide with winters following low fall heat content (2006, 2018 and 2003).

Next, the predictive ability of the fall heat content for the winter mixed layer volume and heat content, or for the maximum seasonal ice volume was tested (Figure 5, bottom panel). Again, the fall heat content is not statistically related to any of these three parameters. Winters 2010 and 2021, which show low sea ice cover and high remaining heat content in March, were both preceded by near-average fall heat content. Winters 2003 and 2014, which are characterized by more sea ice and lower winter mixed layer heat
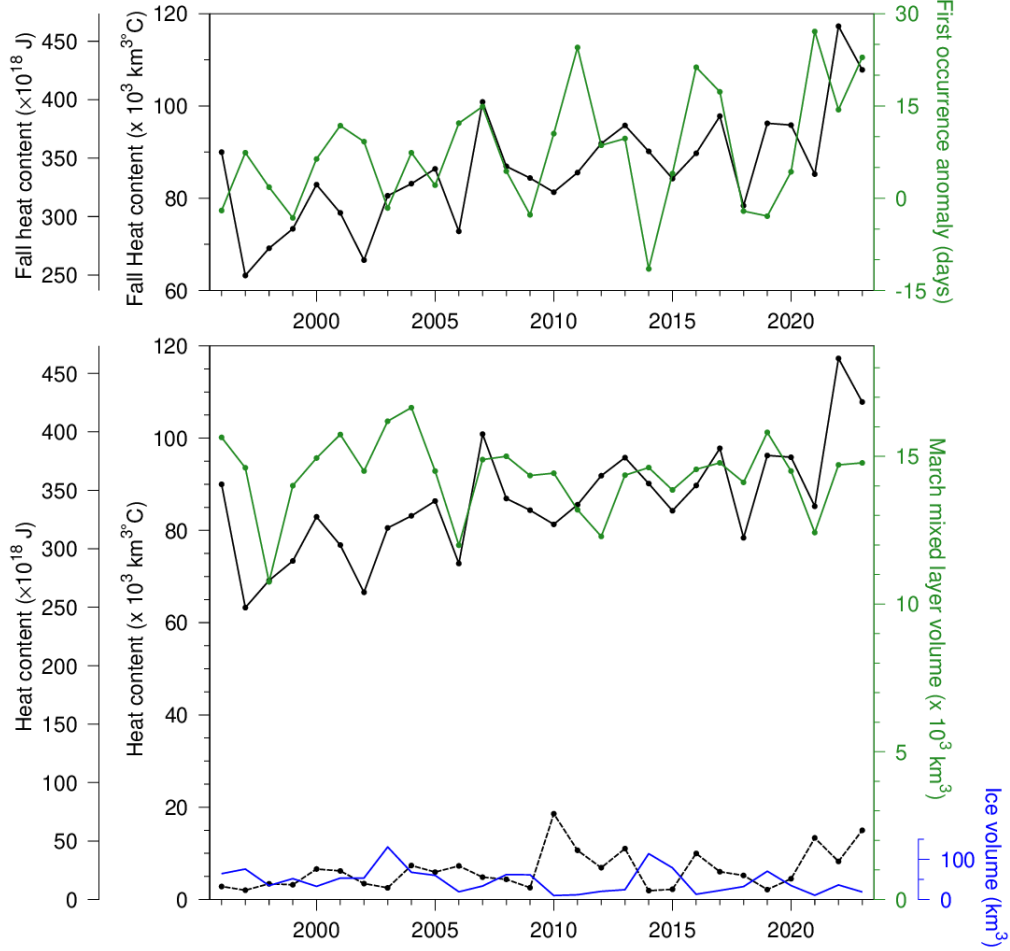
Figure 5. Heat content in the Gulf of St. Lawrence. (Top) Heat content observed during the fall oceanographic survey in the volume occupied by the following March surface mixed layer (black line) and the spatial average of the day of the first occurrence of sea ice anomaly grid (green line). Years are referenced to March (i.e. Fall 2020 is shown at 2021). (Bottom) Same fall heat content as above (black line) compared to March mixed layer volume ($T < 0°$C; green line), March surface mixed layer heat content (black dashed line), and the heat removed for the formation of the maximum observed weekly volume of sea ice (blue line). Ice volume is scaled according to the latent heat of fusion required for its formation.

content than average, were also preceded by near-average fall heat content. The exceptionally high fall heat content that preceeded winter 2022 did not coincide with high March heat content or record low sea ice volume. Figure 5 also shows that the interannual variability in the heat content of the March surface mixed layer is not driven by differences in its volume, the two being weakly correlated.

5 Sea surface temperature coupling to air temperature

Galbraith et al. (2012) showed that the May-to-November monthly climatology of sea surface temperature averaged over the Gulf of St. Lawrence was nearly identical to that of air temperature lagged by half a month. This is shown in Figure 6 using updated datasets and climatology, which here covers the period 1991-2020. From spring to the seasonal maximum sea surface temperature in August, the atmosphere remains warmer than the surface waters and warms them. The opposite occurs once the seasonal maximum is reached when the atmosphere becomes cooler and cools them. This tight interrelation, at least in a climatological sense, informs on the role played by the sensible heat flux, which is a first-order mechanism affecting surface conditions. The sensible heat flux can be estimated by the bulk aerodynamic formulae $Q_s = \rho_a C_{pa} C_H |U| (\text{SST} - T_a)$, where ρ_a is the air density, C_{pa} is the specific heat of air, C_H is the sensible heat transfer coefficient (e.g. MacIntyre et al., 2002) and U is the wind velocity. Since it is proportional to air and water temperature difference, it increases as the air gets warmer than surface waters in spring, and, at some temperature difference given average wind speeds, may become large enough to warm the surface waters at the same rate as the air temperature and to maintain a nearly constant near-surface temperature difference. This is in spite of sensible heat flux being a smaller contribution to the overall heat budget than solar radiation during the summer season. The reverse same situation occurs in the fall except that the mixed layer thickens as the season progresses, increasing the required heat flux to reach equilibium and therefore the temperature difference between air and water. Galbraith et al. (2012) have shown that this strong coupling holds interannually, with the April-November Gulf average air temperature correlated with the May-November sea surface temperature (1982-2010). An analysis using the updated time series over the years 1982 to 2022 finds that the two are correlated with $R^2 = 0.73$.

This strong coupling is likely responsible for the low correlation between fall water column heat content and either the timing of the onset of sea ice, the maximum volume of sea ice formed, or the remaining water column heat content in March. Whatever the initial fall heat content within the water column might be, the ocean surface temperature generally follows the air temperature with a half-month lag: it remains well above freezing if the air temperature stays anomalously warm, or cools rapidly if air temperature cools rapidly. When air temperatures fall below freezing, with water temperature bound by its freezing point, the temperature difference and sensible heat flux both increase to reach values much greater than observed in other seasons. Therefore the timing of the first sea ice occurrence (and subsequent sea ice and winter mixed layer conditions) is only expected to be influenced by the date at which the air temperature falls below the freezing point of seawater, triggering sea ice production, rather than by the warmer air temperature experienced the previous fall. To partly demonstrate this, the relation between air temperature and the DOY when SST reaches a threshold of 0°C in the Northwest Gulf, and with the DOY of the first sea ice occurrence, are explored.

Figure 7 A shows the comparison between the DOY of the first ice occurrence in the Northwest Gulf and the DOY when SST of 0°C is reached on average within the region, based on twice weekly shipborne thermosalinograph transects (see the delimitation of the Northwest Gulf area in Figure 1). Results show that the timing of SST dipping below 0°C explains 73% of the variance of the very first occurrence of sea ice, with a lag of about 20 days when the threshold is crossed early in December, diminishing to 15 days by January 1st. The very first occurrence of sea ice is defined here as the vol-
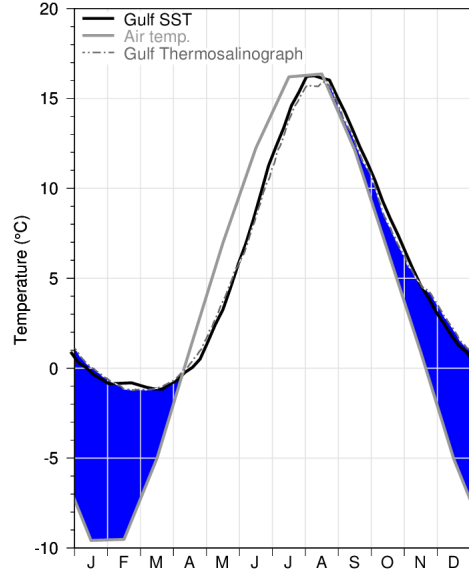
Figure 6. Sea surface and air temperature climatological seasonal cycle in the Gulf of St. Lawrence. AVHRR temperature weekly averages for 1991-2020 are shown (thick black line) as well as thermosalinograph averages (2000-2020; gray dashed line) and monthly air temperature averaged over 13 stations in the Gulf of St. Lawrence for 1991-2020 (thick gray line). The area in blue highlights water and air temperature differences when air is colder than water. See Figure 1 for weather station locations.

ume within the region crossing the threshold of 5% of the largest volume ever recorded in the region. When the analysis is done using the spatially averaged DOY of first occurrence, i.e. the spatial average of the DOY of the first ice occurrence at all grid points in the region in Fig. 2, the variance explained increases slightly to 78% (Figure 7 B). The first occurrence of sea ice is thus well predicted with a few weeks of lead time by the timing of SST reaching 0°C.

The next step is the link to air temperature. The same DOY time series for SST dipping below 0°C is compared first in Figure 7 C to the DOY for air temperature at 2 m dipping below -1.8°C at the NCEP grid point closest to the Northwest Gulf area. The NCEP air temperature time series was first filtered with a 15-day moving average. The relation explains 54% of the variance with a lag of about 3 weeks. Next, in Figure 7 D, the SST DOY time series is compared to the average November-December temperature at the Sept-Îles station. The variance explained increases to 63%, but at the cost of decreased forecast time since the metric isn't available before the end of December. Combining the steps of linking first occurrence of ice directly to these air temperature metrics (Figure 7 E and F) decreases the explaining variance somewhat, but not by very much. The DOY of air temperature falling below the freezing point of salt water (-1.8°C) explains 47% of the variance with a lag of about 40 days. If the sea hasn't occurred by January 1st, the November-December air temperature at Sept-Îles can be used with increased predictability (60%).

6 Sea ice conditions and their relation to winter air temperature

Sea ice production is related to winter atmospheric conditions (air temperature, winds) and ocean mixed layer dynamics. As stated earlier, the striking similarity between
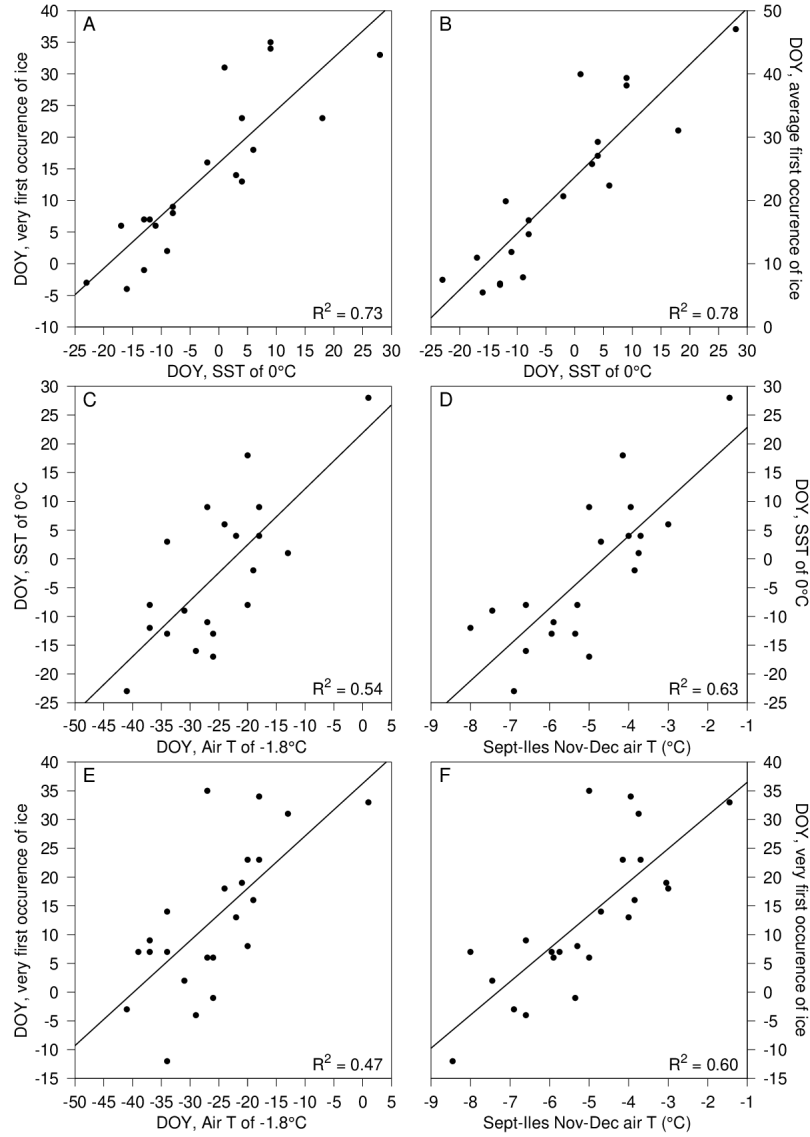
Figure 7. Analysis of first occurrence of sea ice in the Northwestern Gulf. (A and B) Comparison between the date of first occurrence of ice in the Northwestern Gulf and the date when SST of $0°C$ is reached on average within the region, based on twice weekly shipborne thermosalinograph transects (2001-2023, excl. 2010, 2014, and 2015 for which there are no SST data within the time range). In panel A, the very first occurrence of ice is shown, defined as the DOY when the volume reaches 5% of the largest volume ever recorded in the region; this is from Figure 27 of Galbraith et al. (2023) updated to include up to 2023. In panel B, the spatial average of first occurrence of ice is shown, defined as the average anomaly at every grid point of maps such as in Fig. 2 plus the climatological mean in the area delimited as in Figure 1. (C and D) Comparison of SST date from A and B with (C) DOY of air temperature falling below $-1.8°C$ at the closest NCEP grid point, with a 15-day moving average applied to the air temperature time series, and (D) with the average November-December air temperature at the Sept-Îles station. (E and F) Comparison of DOY of very first occurrence of ice with the same air temperatures parameters as in C and D.
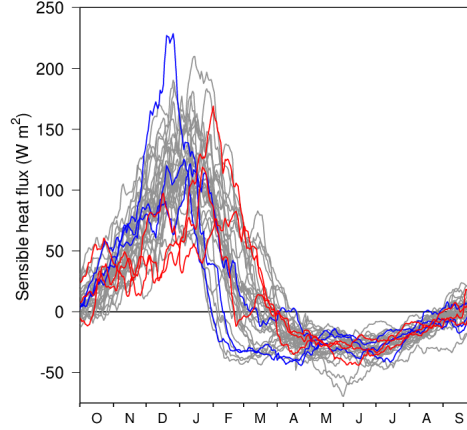
Figure 8. Sensible heat net flux from the NCEP/DOE AMIP-II Reanalysis (Reanalysis-2) with daily averages of 5 grid points in the Gulf of St. Lawrence, filtered using a 31-day running mean (1990-2023). Years are shown from October to October to highlight the winter mixed layer formation period. Years with the highest maximum seasonal ice volume (2003, 1993, and 2014) are shown in blue, years with the lowest maximum seasonal ice volume (2010, 2021, and 2011) are shown in red, and all others are in gray.

May-November surface air temperature and SST suggests a tight coupling through sensible heat flux. This coupling must intensify when air temperatures drop below the freezing point of sea water, increasing the air-sea temperature difference and sensible heat flux. Fig 8 displays the net sensible heat flux extracted from the NCEP dataset and averaged over the five grid points covering the Gulf of St. Lawrence. On average, sensible heat flux accounts for about half of the heat budget in January (100 W versus 200 W), with latent heat flux accounting for most of the remainder. Sensible heat flux decreases quickly in February, more so in high sea ice years (shown in blue) than in low ice years (shown in red) because of the limited area of open water. Surprisingly, this data set shows sensible heat flux becoming negative as early as the end of January in 1993 (blue line with the earliest crossing to negative values) in spite of air temperatures in February 1993 being 5.3°C below the 1991-2020 climatology (and the third coldest month of February on record since 1873, with the coldest being 1923 and 1914 with 6.3 and 5.9 °C below the 1991-2020 climatology, respectively).

In order to find the simplest descriptor of the integrated heat flux variability that can affect the formation of the winter mixed layer and sea ice cover, the blue shaded area in Fig. 6 was investigated, i.e. when the air temperature is colder than water temperature in the climatology. Because SST is close to 0°C between December and March, when the air-water temperature difference is largest, the area in blue representing the air-water temperature difference intrinsic to the sensible heat flux is well approximated by the average winter air temperature (DJFM). This metric is shown in Fig. 4 (blue line) and is highly correlated with all sea ice metrics, with R^2 values ranging from 0.75 to 0.83.

7 Discussion and summary

The spring-to-summer sea surface temperature averaged over the Gulf of St. Lawrence is similar to that of air temperature lagged by a half-month, suggesting strong coupling between the two through sensible heat flux. Perhaps counter-intuitively, because of this strong coupling, the early fall heat content in the volume that will eventually become

R^2 Table	Ice max volume (1969-2023)	Ice Duration (1969-2023)	DJFM air temp (1969-2023)	DJF air temp (1969-2023)	DJ air temp (1969-2023)
Ice max area (1969-2023)	0.80	0.84	0.81	0.84	0.64
Ice max volume (1969-2023)		0.78	0.75	0.73	0.50
Ice Duration (1969-2023)			0.83	0.84	0.74
DJFM air temp (1969-2023)				0.92	0.67
DJF air temp (1969-2023)					0.80

Figure 9. Correlation coefficients (R^2) for regressions between sea ice and air temperature time series for the Gulf of St. Lawrence. All are statistically significant ($p < 0.05$; autocorrelation of the time series is not considered to reduce the number of degrees of freedom).

occupied by the winter mixed layer is not an important driver of the date of the first occurrence of sea ice in the Gulf of St. Lawrence. Only the time period when air and water temperature get close to freezing is decisive. The first occurrence of sea ice was shown to occur about 15 to 20 days after SST reaches an average of 0°C in the Northwest Gulf, with the lag decreasing later in the season. The first occurrence of sea ice was shown to occur about 40 days after air temperature dips below -1.8°C, with less variance explained in the forecast (from 73-78% using SST to 47% using air temperture).

Figure 9 shows the correlation coefficient (R^2) matrix between various sea ice seasonal maximum and duration metrics against air temperature in the Gulf of St. Lawrence. Once the surface water is limited by the freezing point, which is close to 0°C, the sensible heat flux reaches its maximum values. The average air temperature then acts as a proxy for the difference between the sea surface and air temperatures, and sea ice metrics become strongly correlated with the mean air temperature for the December to March (DJFM) period. This relationship most likely operates through the sensible heat flux. Correlations are also high (and in some cases higher) against the average air temperature observed between December and February (DJF). In years of very light sea ice cover, the maximum often occurs early, in February, making the March temperatures moot (although very cold March temperatures might have delayed the maximum). In years of very high sea ice cover, the Gulf is mostly ice-covered by March, which reduces the area over which sea-air heat flux can occur, making the March temperatures a less useful predictor of average sensible heat flux. It is therefore not surprising that the DJF average air temperature proved to be a slightly better predictor than the DJFM average air temperature for two of three sea ice parameters. In spite of reduced sensible heat fluxes often observed in February (Fig. 8), removing this month from the averaging period (leaving only December and January) leads to still statistically significant but much reduced correlations, between 0.50 and 0.74 down from between 0.73 and 0.84.

The average winter air temperature is a very good predictor of sea ice conditions metrics, with linear relations indicating losses of 18 km^3, 31 000 km^2 and 14 days of the sea ice season for each 1°C increase in DJFM air temperature (R^2 of 0.75, 0.81 and 0.83 respectively) and of 17 km^3, 30 000 km^2 and 13 days of sea ice season for each 1°C increase in DJF air temperature (R^2 of 0.73, 0.84 and 0.84 respectively). While climate change projections usually need to extrapolate outside of the observed variability to forecast near-zero conditions, the observations since 1969 include the near absence of sea ice and are thus within the bounds of interpolation.
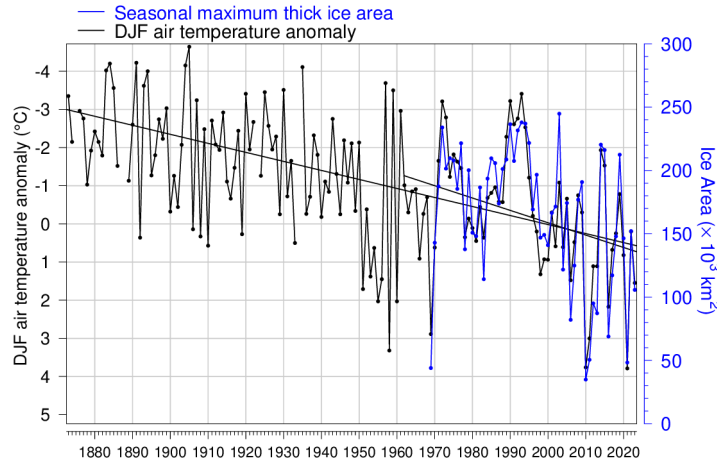
Figure 10. Seasonal maximum ice area and December-to-February (DJF) air temperature anomaly relative to 1991-2020 climatology, averaged over meteorological around the Gulf of St. Lawrence. Black lines show linear regressions for two periods. The 1873-2023 trend in air temperature is 2.3°C per 100 years and 1962-2023 is 3.2°C per 100 years but is not statistically different at 95% confidence intervals.

Figure 10 shows the long-term average DJF temperature anomaly from all available meteorological stations back to 1873, when only 3 stations were available. A warming trend of 2.3°C per 100 years is observed superimposed on a high interannual variability. Only five winters had DJF temperature anomalies greater than 2.9°C in that period, and DJFM temperature anomalies greater than 2.4°C, and they all coincide with the only winters that were nearly ice-free in the Gulf of St. Lawrence. These are recorded in our sea ice dataset as 1969, 2010, 2011 and 2021. To those four years is added 1958 for which sea ice was reported to extend eastward to only just East of Prince Edward Island and the Western end of Anticosti Island (Black, 1958), resembling conditions of 2021. Prior to 1958, no winters were likely to have been sufficiently warm to lead to nearly ice-free conditions in the Gulf. However, the Gulf of St. Lawrence has since entered a period with occasional nearly ice-free winters, a condition that is expected to become more common in the near future. Note that the term used here is "nearly ice-free" condition because the coastal areas and shallow bays that freeze up early (Figure 2) will likely remain at least occasionally ice-covered in spite of warming for far longer. This temperature anomaly threshold is similar to that of 2 to 4°C found for various regions of the Sea of Okhotsk by Takahashi et al. (2011), also using the correlation between winter air temperature and sea ice extent.

The more recent warming trend (1962-2023) in winter air temperatures of 3.2°C per 100 years (Figure 10) hints at being steeper than the entire series trend but is not statistically different at 95% confidence intervals. If a 2 to 3°C per 100 years trend is maintained, winter air temperatures will reach an average of 2.4°C warmer than the 1991-2020 climatology after about 100 years; earlier if the warming rate increases as the trend over the more recent period suggests and as climate models project (see below). But even then, interannual variability in air temperature associated with weather patterns, e.g. the polar vortex, will continue to drive interannual variability in sea ice. In the early 1990s, DJF average air temperatures were about 3°C colder than the long-term trend. If colder than normal temperatures of this magnitude still occur on occasion, it might take another 100 years for the Gulf to become permanently ice-free except for coastal ice.

However, this discussion hinges on the temperature anomaly threshold that distinguishes the years with nearly no ice cover, while these years were also characterized by a winter mixed layer that was significantly warmer than required to prevent ice formation. In March 2010, for example, the mixed layer was 1°C above freezing over the Magdalen Shallows and over 2°C above freezing on the Southeastern area between the coast of Newfoundland and Anticosti Island (Figure 3). Perhaps a year such as 2016 is more relevant, when the mixed layer was overall 1°C cooler and near-freezing over the Magdalen Shallows, with sea ice that had just started to form (Figure 3). The DJF winter air temperature anomaly was then of +2.2°C (Figure 10), the next warmest after the five nearly ice-free winters, a threshold that could be reached two to three decades sooner in the long-term trend.

These projections are consistent with some aspects of recent numerical modelling results. Perrie et al. (2015) investigated the effects of IPCC SRES scenario A1B that assumes increasing carbon dioxide emissions until around 2050 and decreasing thereafter, which is a moderate emission scenario similar to RCP6.0. Using downscaling projections over the Gulf, they found winter air temperatures increases of 2.5 to 3.5°C by 2040-2069 and of 4 to 5°C by 2070-2099 relative to 1970-1999. We must reduce these increases by 0.8°C to account for our already warmer 1991-2020 climatology (based on our 13-station average time series). This is slightly faster warming than the current rate. Long et al. (2016) modelled sea ice changes in the Gulf using the same IPCC scenario and obtained a crossing of the interannual mean sea ice conditions through zero by 2069, leaving interannual variability to create some ice in colder than normal years. This is also slightly faster than the current rate but is consistent with the increase in winter air temperature of 2 to 3° averaged over the Gulf. Note that their modelled sea ice volume time series exhibits much less interannual variability than our observations and does not show the near absence of sea ice that has already occurred before the 2050s. We speculate that the relatively thin winter mixed layer in the model leads to easier production of sea ice. Indeed some numerical models obtain a sea ice cover under current climate conditions that are similar to observations, but with a much thinner winter mixed layer thickness, casting doubt on their ability to predict future climates given the assumed influence of the oceanic surface mixed layer on sea ice conditions. The winter depth of the 0°C isotherm modelled by Long et al. (2016) reaches only about 40 m in the center of the Gulf instead of the much deeper observations (see their Fig. 7). Saucier et al. (2003) also successfully simulated the sea ice cover to within error bars of observations, while simultaneously underestimating the volume of the surface mixed layer ($T < 0$°C) to only 7000 km^3, or less than half the volume typically observed (Fig. 5).

While numerical modelling can be a very useful tool to forecast sea ice conditions in the Gulf of St. Lawrence that will be associated with climate change, they currently have limitations in correctly modelling the present winter mixed layer. Therefore studies such as the present one based on understanding observations, quantifying variability, and identifying simple relations between forcings and observed conditions are complementary and valuable, allowing the use of past variability to forecast conditions associated with anticipated changes in climate.

The Gulf of St. Lawrence has a winter mixed layer that is comparably thick (average of 75 m; Galbraith, 2006) with respect to typical values in the Arctic basins (Peralta-Ferriz & Woodgate, 2015). It may thus be somewhat surprising to reach the conclusion that interannual sea ice metrics are driven by atmospheric temperature variability, similarly to the Sea of Okhotsk (Takahashi et al., 2011), rather than by ocean heat content. In the Arctic Ocean, the prediction of the minimum conditions in September face what has been termed a June 1st "spring barrier" (Bonan et al., 2019) whereby the variability of onset of melt limits forecasts before that date. In the Gulf of St. Lawrence, the first occurrence of sea ice and the overall seasonal ice severity cannot be predicted by the heat content in early fall as it is lost to the atmosphere quickly enough in any case

when air temperatures fall below freezing. The November-December air temperature in the Northwest Gulf predicts first occurrence of sea ice in that area, and the overall Gulf sea ice cover severity for the season (as determined by duration and by maximum area and volume) are highly correlated with January-February or January-March air temperatures, yielding relations that are useful for assesments of climate change impacts (e.g. losses of 18 km^3, 31 000 km^2 and 14 days of the sea ice season for each 1°C increase in DJFM air temperature). Five nearly ice-free winters correspond to the warmest December to February (or December to March) average air temperatures over the Gulf, from which we infer a warming of 2.2 to 2.4°C above the 1991-2020 climatology leads to nearly ice-free conditions in the Gulf of St. Lawrence.

Open Research Section

Sea ice charts were downloaded from the Canadian Ice Service web site on its Archive section. Heat flux data and daily surface air temperature were extracted from the NCEP Reanalysis 2 open dataset, provided by the NOAA/OAR/ESRL Physical Sciences Laboratory (Boulder, Colorado, USA). Monthly air temperature averages from Environment and Climate Change Canada (ECCC) and were downloaded from the Adjusted and Homogenized Canadian Climate Data (AHCCD) web site. The Ship thermograph data and the Fall and March water column temperature and salinity profiles are from Fisheries and Oceans Canada's Atlantic Zone Monitoring Program (AZMP) and are available by request to Fisheries and Oceans Canada's Marine Environmental Data at https://www.meds-sdmm.dfo-mpo.gc.ca/isdm-gdsi/request-commande/form-eng.asp These data are in the process of being made available through the Canadian Integrated Ocean Observing System (CIOOS) web portal.

Acknowledgments

References

Arthun, M., Onarheim, I. H., Dörr, J., & Eldevik, T. (2021). The seasonal and regional transition to an ice-free arctic. *Geophysical Research Letters*, *48*(1), e2020GL090825. doi: https://doi.org/10.1029/2020GL090825

Black, W. A. (1958). Gulf of St. Lawrence ice survey, winter 1958. *Geographical Branch, Ottawa, Geographical Paper*, *19*, 26 pp.

Blockley, E. W., & Peterson, K. A. (2018). Improving met office seasonal predictions of arctic sea ice using assimilation of CryoSat-2 thickness. *The Cryosphere*, *12*(11), 3419–3438. doi: 10.5194/tc-12-3419-2018

Bonan, D. B., Bushuk, M., & Winton, M. (2019). A spring barrier for regional predictions of summer Arctic sea ice. *Geophysical Research Letters*, *46*(11), 5937-5947. doi: https://doi.org/10.1029/2019GL082947

Bonan, D. B., Schneider, T., Eisenman, I., & Wills, R. C. J. (2021). Constraining the date of a seasonally ice-free arctic using a simple model. *Geophysical Research Letters*, *48*(18), e2021GL094309. doi: https://doi.org/10.1029/

2021GL094309

Brickman, D., Wang, Z., & DeTracey, B. (2016). High resolution future climate ocean model simulations for the Northwest Atlantic Shelf region. *Canadian Technical Report of Hydrography and Ocean Sciences*, *315*, 143 pp.

Cyr, F., Bourgault, D., & Galbraith, P. S. (2011). Interior versus boundary mixing of a cold intermediate layer. *J. Geophys. Res.*, *116*(C12029). doi: 10.1029/ 2011JC007359

Cyr, F., Snook, S., Bishop, C., Galbraith, P., Chen, N., & Han, G. (2022). Physical oceanographic conditions on the Newfoundland and Labrador Shelf during 2021. *DFO Can. Sci. Advis. Sec. Res. Doc.*, *2022/040*, iv + 48 p.

Déry, F. (1992). Interannual and intraseasanal variability of the ice cover in the Gulf of Saint Lawrence, 1963-1990. *McGill University, M.Sc. Thesis*, 220 pp.

DeTracey, B. (1993). Modelling interannual sea ice variabiiity in the Gulf of St. Lawrence. *McGill University, M.Sc. Thesis*, 108 pp.

Galbraith, P. S. (2006). Winter water masses in the Gulf of St. Lawrence. *J. Geophys. Res.*, *111*, C06022. doi: 10.1029/2005JC003159

Galbraith, P. S., Chassé, J., Shaw, J.-L., Dumas, J., Lefaivre, D., & Bourassa, M.-N. (2023). Physical oceanographic conditions in the gulf of st. lawrence during 2022. *Can. Tech. Rep. Hydrogr. Ocean Sci.*, *354*, v + 88 p.

Galbraith, P. S., Larouche, P., & Caverhill, C. (2021). A sea-surface temperature homogenization blend for the Northwest Atlantic. *Canadian Journal of Remote Sensing*, *47:4*, 554-568. doi: 10.1080/07038992.2021.1924645

Galbraith, P. S., Larouche, P., Chassé, J., & Petrie, B. (2012). Sea-surface temperature in relation to air temperature in the Gulf of St. Lawrence: interdecadal variability and long term trends. *Deep-Sea Res. II*, *77-80*, 10-20.

Galbraith, P. S., Saucier, J., Michaud, N., Lefaivre, D., Corriveau, R., Roy, F., . . . Cantin, S. (2002). Shipborne monitoring of near-surface temperature and salinity in the Estuary and Gulf of St. Lawrence. *Atlantic Zone Monitoring Program Bulletin*(2), 26-30.

Gilbert, D., & Pettigrew, B. (1997). Interannual variability (1948-1994) of the CIL core temperature in the Gulf of St. Lawrence. *Canadian Journal of Fisheries and Aquatic Sciences*, *54*(S1), 57–67. doi: 10.1139/cjfas-54-S1-57

Lavoie, D., Lambert, N., Rousseau, S., Dumas, J., Chassé, J., Long, Z., . . . Azetsu-Scott, K. (2020). Projections of future physical and biogeochemical conditions in the Gulf of St. Lawrence, on the Scotian Shelf and in the Gulf of Maine. *Canadian Technical Report of Hydrographic and Ocean Sciences*, *334*, xiii + 102 p.

Li, Y. (2000). Intraseasonal and interannual variability of sea ice in the Gulf of St. Lawrence. *McGill University, Ph.D. Thesis*, 188 pp.

Long, Z., Perrie, W., Chassé, J., Brickman, D., Guo, L., Drozdowski, A., & Hu, H. (2016). Impacts of climate change in the gulf of st. lawrence. *Atmosphere-Ocean*, *54*(3), 337-351. doi: 10.1080/07055900.2015.1029869

MacIntyre, S., Romero, J. R., & King, G. W. (2002). Spatial-temporal variability in surface layer deepening and lateral advection in an embayment of Lake Victoria, East Africa. *Limol. Oceanogr.*, *47*(3), 656-671. doi: 10.4319/lo.2002.47.3.0656

Notz, D., & SIMIP Community. (2020). Arctic sea ice in CMIP6. *Geophysical Research Letters*, *47*(10), e2019GL086749. doi: https://doi.org/10.1029/ 2019GL086749

Pellerin, P., Ritchie, H., Saucier, F. J., Roy, F., Desjardins, S., Valin, M., & Lee, V. (2004). Impact of a two-way coupling between an atmospheric and an ocean-ice model over the gulf of st. lawrence. *Monthly Weather Review*, *132*(6), 1379-1398. doi: https://doi.org/10.1175/1520-0493(2004)132⟨1379: IOATCB⟩2.0.CO;2

Peralta-Ferriz, C., & Woodgate, R. A. (2015). Seasonal and interannual vari-

ability of pan-Arctic surface mixed layer properties from 1979 to 2012 from hydrographic data, and the dominance of stratification for multiyear mixed layer depth shoaling. *Progress in Oceanography*, *134*, 19-53. doi: https://doi.org/10.1016/j.pocean.2014.12.005

Perrie, W., Long, Z., Chassé, J., Blokhina, M., Guo, L., & Hu, H. (2015). Projected changes in surface air temperature and surface wind in the gulf of st. lawrence. *Atmosphere-Ocean*, *53*(5), 571-581. doi: 10.1080/07055900.2015.1086295

Saucier, F., Roy, F., Gilbert, D., Pellerin, P., & Ritchie, H. (2003). Modeling the formation and circulation processes of water masses and sea ice in the Gulf of St. Lawrence, Canada. *J. Geophys. Res.*, *108 (C8)*, 3269. doi: 10.1029/2000JC000686

Senneville, S., & Saucier, F. J. (2007). Étude se sensibilit'e de la glace de mer au réchauffement climatique dans le Golfe et l'estuaire du Saint-Laurent. *Report to Ouranos*, 30 pp.

Shaw, J.-L., & Galbraith, P. S. (2023). Climatology of transport in the Strait of Belle Isle. *J. Geophys. Res.*, *128*(e2022JC019084). doi: 10.1029/2022JC019084

Smith, G. C., Roy, F., & Brasnett, B. (2013). Evaluation of an operational ice-ocean analysis and forecasting system for the Gulf of St Lawrence. *Quarterly Journal of the Royal Meteorological Society*, *139*(671), 419-433. doi: https://doi.org/10.1002/qj.1982

Takahashi, S., Kosugi, T., & Enomoto, H. (2011). Sea-ice extent variation along the coast of Hokkaido, Japan: Earth's lowest-latitude occurrence of sea ice and its relation to changing climate. *Annals of Glaciology*, *58(58)*. doi: 10.3189/172756411797252301

Therriault, J., Petrie, B., Pepin, P., Gagnon, J., Gregory, D., Helbig, J., ... Sameoto, D. (1998). Proposal for a northwest zonal monitoring program. *Canadian Technical Report of Hydrographic and Ocean Sciences*, *194*, vii + 57 p.

Urrego-Blanco, J., & Sheng, J. (2014). Formation and distribution of sea ice in the Gulf of St. Lawrence: A process-oriented study using a coupled ocean-ice model. *J. Geophys. Res.*, *119*, 7099-7122. doi: 10.1002/2014JC010185

Vincent, L. A., Wang, X. L., Milewska, E. J., Wan, H., Yang, F., & Swail, V. (2012). A second generation of homogenized Canadian monthly surface air temperature for climate trend analysis. *J. Geophys. Res.*, *117*(D18). doi: 10.1029/2012JD017859

WMO. (2017). WMO guidelines on the calculation of climate normals. *Tech. rep., Geneva, Switzerland*, *WMO-No. 1203*, 29 p.